JACS
JOURNAL OF THE AMERICAN CHEMICAL SOCIETY
pubs.acs.org/JACS
Article

High-Density Palladium Single-Atom Catalysts for Photoinduced Tandem Decarbonylation/Carbonylative Reductive Coupling

Haolin Du,‡ Qi Yu,‡ Yucong Miao, Junli Ao, Jiale Wu, Kun Fu, Yang Shi, Jun Li,* Jun-An Ma,* and Jie Wu*

Cite This: https://doi.org/10.1021/jacs.5c12630
Read Online

ABSTRACT: In carbonylation reactions, a carbonyl source is typically required, often supplied by carbon monoxide (CO) gas or CO surrogates that release CO via decarbonylation. Herein, we report a novel carbonylative reductive coupling reaction utilizing pivaldehyde as a facile and cost-effective carbonyl source with water serving as an environmentally benign reductant. A polymeric carbon nitride semiconductor functionalized with high-density single-atom palladium was designed as a multifunctional catalytic system, simultaneously driving a cascade decarbonylation−CO migration−carbonylative coupling process while enabling photocatalytic water oxidation to supply electrons for the reductive coupling. Life cycle assessment analysis further supports the economic viability of our carbonylative reductive coupling strategy. The spatial proximity of Pd atoms is crucial in promoting efficient CO migration, and computational studies offer atomic-level insights into this high-density configuration in the reaction. The heterogeneous single-atom photocatalyst exhibits exceptional stability, maintaining its catalytic activity over 10 consecutive cycles with minimal loss in performance. The practical utility of this method was demonstrated through the efficient synthesis of pharmaceutical compounds, including a decagram-scale synthesis of AdipoRon in a high-speed circulation flow system. This work seamlessly integrates decarbonylation, photocatalytic water splitting, and reductive coupling reactions, underscoring the tremendous potential of single-atom photocatalysts in advancing sustainable cascade organic transformations.

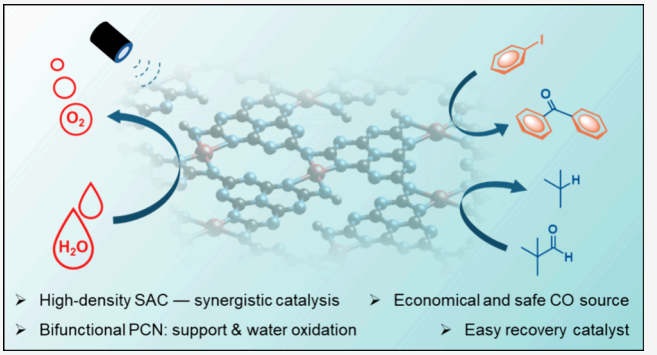

INTRODUCTION

Carbonyl compounds represent one of the most fundamental and versatile classes of functional groups in organic synthesis, serving as essential building blocks in the construction of natural products and biologically active compounds.[1−5] Classic synthetic methods are based on the transformation of existing functional groups, such as the oxidation of alcohols to ketones, the conversion of carboxylic acid derivatives, and the Friedel−Crafts acylation reaction of arenes with acyl chlorides. In addition to these well-established methodologies, multicomponent cross-coupling reactions with a carbonyl source can also be employed to synthesize these types of carbonyl compounds. Since Heck et al.'s groundbreaking research in the 1970s, multicomponent carbonylation reactions involving the direct participation of carbon monoxide gas have gradually become one of the most practical strategies for constructing carbonyl compounds.[6−10] For instance, in the presence of CO gas, the coupling reactions of alkyl or aryl halides with nucleophiles (such as alcohols, amines, and organometallic compounds) are extensively studied (Figure 1A).[11−18]

Despite the high efficiency of CO gas in carbonylation reactions, its widespread application remains limited due to significant safety concerns. This is largely due to the toxic nature of CO, which can inhibit oxygen binding to hemoglobin and lead to asphyxiation. Additionally, CO is invisible, odorless, and tasteless, necessitating stringent handling protocols, including specialized storage, transport, and the use of CO detectors and high-pressure equipment.[19,20] To mitigate these risks, various CO precursors have been developed that can generate CO gas under specific conditions, such as formic acid and its derivatives, oxalic acid, oxalyl chloride, and metal carbonyl compounds.[21−29] Furthermore, commercially available CO surrogates have been engineered to degrade through different mechanisms in a controlled manner, supplying CO gas to carbonylation reactions *ex situ*, such as COgen,[30] carboxyboronate,[31] CO-501,[32] TFBen,[33,34] etc (Figure 1B).

Received: July 23, 2025
Revised: December 1, 2025
Accepted: December 3, 2025

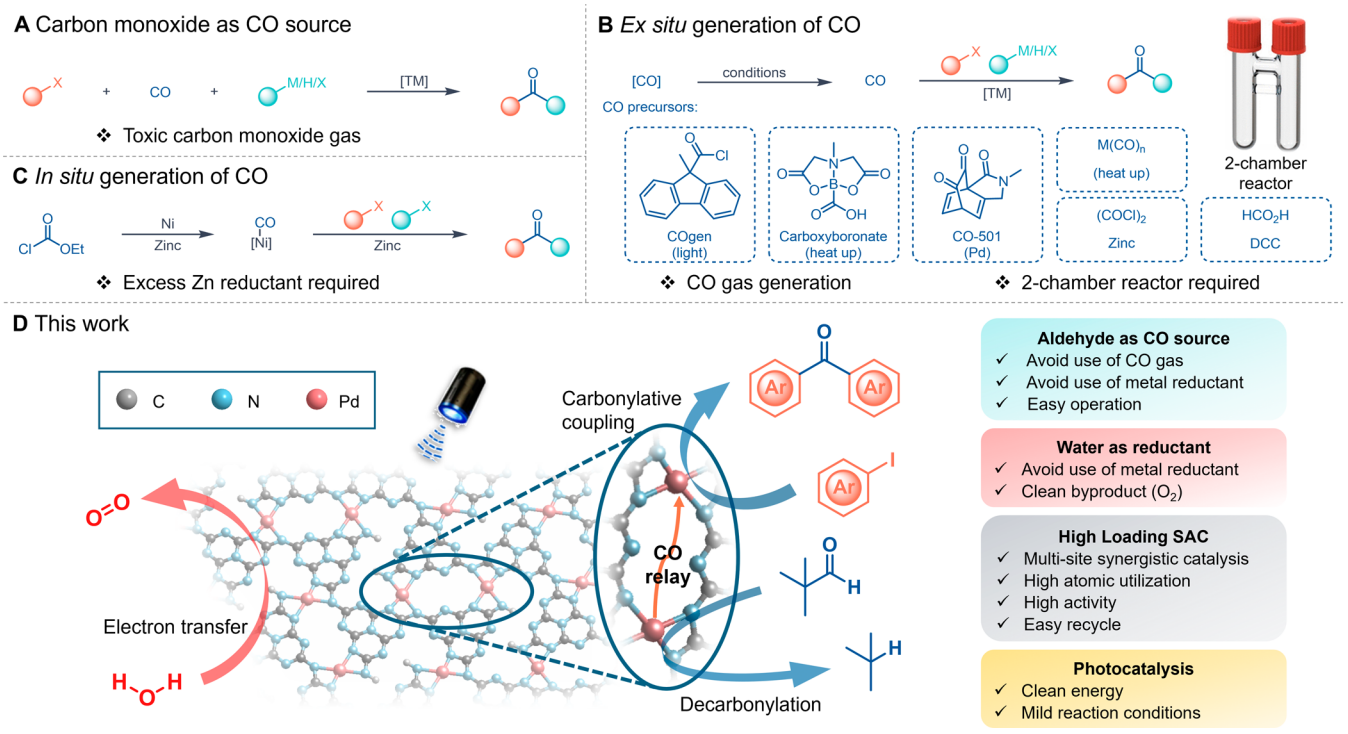

Figure 1. Strategies for incorporating CO in carbonylative coupling reactions. (A) Using CO gas for ketone synthesis. (B) Using CO surrogates for CO generation assisted by a two-chamber reactor. (C) *In situ* decarbonylation−carbonylation reaction. (D) This work: a high-density Pd single-atom photocatalyst promoted decarbonylation/carbonylative reductive coupling cascade.

Although advancements have been made, the use of CO precursors and surrogates presents certain challenges. Specifically, decarbonylation and carbonylation are not synchronous, necessitating an excess of CO precursors and leaving substantial residual CO gas in the reactor after the reaction.[19] Additionally, if the conditions for carbonylation and decarbonylation are incompatible, a specialized two-chamber reactor is required.[29,30] To address these limitations, an *in situ* decarbonylation−carbonylation strategy was developed using ethyl chloroformate as the carbonyl source (Figure 1C). In this approach, ethyl chloroformate undergoes oxidative addition with nickel, followed by CO cleavage and reductive elimination, resulting in a metal carbonyl complex in which CO acts as a ligand to bind with nickel. Subsequently, CO insertion happens in the following reductive coupling to obtain the carbonylative product.[35,36] However, this reaction requires excess zinc for the reductive coupling and *in situ* formation of CO, generating redundant chemical waste.

Single-atom catalysts (SACs), consisting of individual metal atoms anchored on a support material, are widely regarded as a bridge between homogeneous and heterogeneous catalysis, owing to their maximized metal atom utilization efficiency and well-defined coordination environments.[37,38] The insoluble nature of the support enables efficient catalyst recovery and recycling, enhancing their sustainability. While SACs have been extensively applied in photocatalysis, particularly for water splitting, their usage in fine chemical organic synthesis remains nascent. Notably, nickel-anchored carbon nitride (CN) photocatalysts have shown exceptional performance in cross-coupling reactions involving C−X bond formations with alcohols,[39,40] amines,[41] and carboxylic acids.[42]

Herein, we report an alternative approach to synthesize ketones through the integration of SAC-mediated water photolysis and a transition-metal-catalyzed decarbonylation/carbonylative reductive coupling cascade. This tandem process involves a light-driven, high-density Pd single-atom-catalyzed carbonylative reductive coupling using inexpensive pivaldehyde as the carbonyl source. This method generates oxygen as the oxidative byproduct and isobutane as the decarbonylation byproduct, both of which are benign and easy to remove. A life cycle assessment (LCA) further underscores the environmental advantages of this strategy. Remarkably, our strategy leverages the unique properties of a high-density Pd single-atom catalyst, where the high metal loading enables synergistic catalysis among neighboring metal centers,[43−47] facilitating efficient decarbonylation, CO migration, and carbonylative coupling. Notably, this heterogeneous catalyst can be easily recovered by simple filtration, with no significant loss of catalytic activity observed over 10 recovery cycles, highlighting the sustainability and practicality of this catalytic approach. This work not only provides a novel and efficient method for carbonylative reductive coupling reactions using water as a green reductant but also discloses the unique catalytic performance of a high-metal-density single-atom photocatalyst (SAPC).

RESULTS AND DISCUSSION

Design, Synthesis, and Characterization of SACs. In designing an efficient SAC for the carbonylative reductive coupling reaction, we identified several critical criteria for the support material: (1) appropriate anchoring sites for transition metal atoms, (2) light absorption capability in the visible and near-UV range with efficient electron−hole separation, (3) suitable valence band position for water oxidation, and (4) commercial availability or facile synthesis from cost-effective precursors. After investigation of various semiconductor materials reported in the literature, polymeric carbon nitride

https://doi.org/10.1021/jacs.5c12630
J. Am. Chem. Soc. XXXX, XXX, XXX−XXX

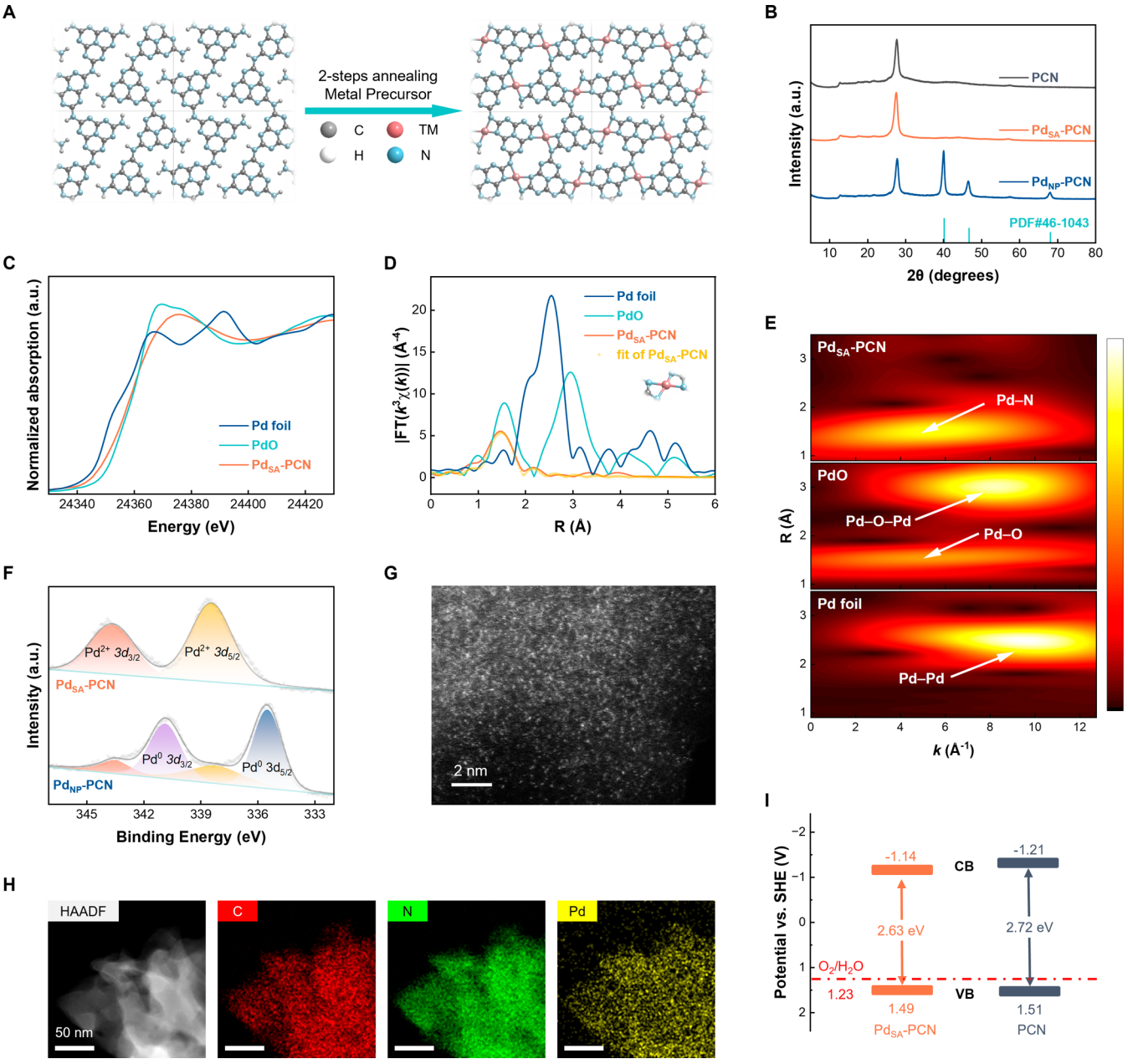

Figure 2. (A) Preparation of the M_{SA}-PCN. (B) XRD spectra of PCN, Pd_{SA}-PCN, and Pd_{NP}-PCN. (C) Pd K-edge XANES spectra of Pd_{SA}-PCN, PdO, and Pd foil. (D) Fourier transform k^3-weighted EXAFS of Pd_{SA}-PCN, PdO, and Pd foil. (E) Wavelet transform k^3-weighted EXAFS of Pd_{SA}-PCN, PdO, and Pd foil. (F) Pd 3d XPS spectra of Pd_{SA}-PCN and Pd_{NP}-PCN. (G) AC-HAADF-STEM image of Pd_{SA}-PCN. (H) HAADF-STEM image and corresponding element mapping of Pd_{SA}-PCN. (I) Band edge position diagrams of Pd_{SA}-PCN and PCN.

(PCN) emerged as an ideal candidate, fulfilling all the aforementioned criteria.[48−52] PCN is characterized by its cost-effectiveness, nontoxicity, and facile synthesis process. Moreover, the PCN subjected to thermal exfoliation exhibits a structure that deviates from that of ideal crystalline PCN and features a significantly higher surface area.[47,53] Its surface presents a variety of nitrogen atoms, including pyridinic nitrogen in triazine units, bridging nitrogen, and terminal amino groups, offering diverse coordination environments for metal anchoring.[54]

The transition metal single-atom supported on PCN (hereafter referred to as M_{SA}-PCN) was synthesized through a two-step annealing process (Figure 2A).[55] The first low-temperature annealing step facilitates controlled ligand removal and selective metal bonding to the support, while the second high-temperature step (500 °C) ensures the complete removal of the remaining chloride ligands. This protocol enables the preparation of ultrahigh-density single-atom catalysts (UHD-SACs) with atomically dispersed transition metal atoms on the PCN support. Inductively coupled plasma−optical emission spectrometry (ICP-OES) analysis confirmed exceptionally high metal loadings, with Pd reaching 19.23 wt %. Additionally, Cu (9.5 wt %) and Ni (8.85 wt %) also achieved remarkable loadings, along with other transition metals as detailed in Table S1.

Figure 2B shows X-ray diffraction (XRD) patterns of PCN, Pd_{SA}-PCN, and Pd_{NP}-PCN. The peaks located at 40.1°, 46.7°, and 68.2° of Pd_{NP}-PCN can be designated as the (111), (200),

https://doi.org/10.1021/jacs.5c12630
J. Am. Chem. Soc. XXXX, XXX, XXX−XXX

Scheme 1. (A–C) Optimization of the Reaction Conditions[a]

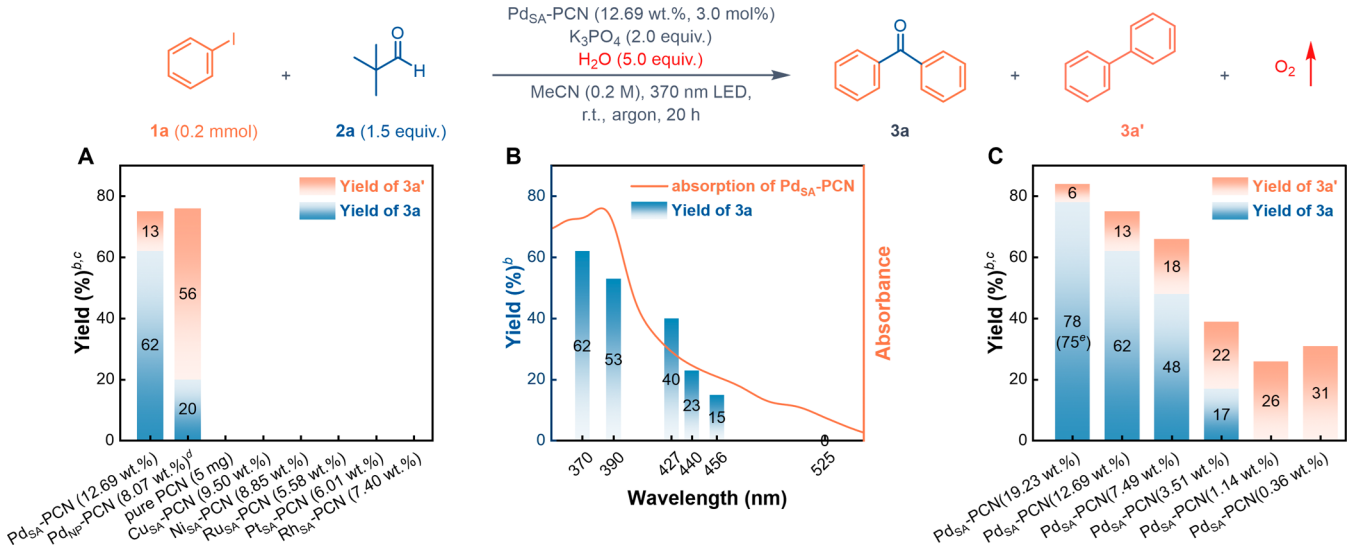

[a]Standard conditions: **1a** (0.2 mmol), **2a** (0.3 mmol, 1.5 equiv), Pd_{SA}-PCN (12.69 wt %, 5.0 mg, 3.0 mol %), K_3PO_4 (85 mg, 2.0 equiv), H_2O (18 μL, 5.0 equiv), MeCN (1.0 mL), 370 nm LED (40 W), 20 h, r.t., under an argon atmosphere. [b]Yields determined by ^1H NMR of the crude reaction mixture, with CH_2Br_2 as an internal standard. [c]The metal atom amount was set at 3.0 mol %. [d]Pd_{NP}-PCN was synthesized according to the literature report.[56] [e]Isolated yield.

(220) facets of Pd metal (PDF# 46-1043), while no obvious peaks of nanoparticles were observed on Pd_{SA}-PCN. XRD patterns for other transition metals (Cu, Ni, Ru, etc.) are presented in Figure S2. The X-ray absorption fine structure (XAFS) analysis provides reliable insights into the electronic structure and short-range coordination environment of Pd in the Pd_{SA}-PCN catalyst. As shown in Figure 2C, the X-ray absorption near edge structure (XANES) spectra reveal that the absorption threshold and white-line intensity of Pd_{SA}-PCN are situated between those of Pd foil and PdO, indicating a positive oxidation state of the Pd atom in Pd_{SA}-PCN. In the k^3-weighted Fourier transform (FT) extended X-ray absorption fine structure (EXAFS), Pd_{SA}-PCN displays a dominant peak at a lower R value (1.4 Å) compared with the PdO standard (1.6 and 3 Å). Moreover, it does not show a significant peak at 2.6 Å, which would correspond to Pd–Pd bonds in the Pd foil reference. According to the fitting of EXAFS, the Pd atoms in Pd_{SA}-PCN are in a 4-coordinate environment with nitrogen atoms (Figure 2D). The wavelet transform (WT) EXAFS analysis further corroborates these findings. Pd_{SA}-PCN shows intensity concentrated at lower R (1.4 Å) and k (5 $Å^{-1}$) values, such signals that are slightly different from the PdO standard (1.6 Å, 6 $Å^{-1}$and 3 Å, 9 $Å^{-1}$). In contrast, the Pd foil reference displays strong intensity at higher R (2.6 Å) and k (10 $Å^{-1}$) values, while it is not significantly observed in Pd_{SA}-PCN (Figure 2E). X-ray photoelectron spectroscopy (XPS) provides information on the oxidation state of Pd (Figure 2F). In Pd_{NP}-PCN, the Pd 3d XPS spectra can be deconvoluted into two pair peaks located at 343.7 and 338.4 eV and 340.9 and 335.5 eV, assigned to Pd^{2+} and Pd^0, respectively. In comparison, only the peak corresponding to Pd^{2+} is detected in Pd_{SA}-PCN, indicating that Pd in Pd_{SA}-PCN exists in a positive oxidation state, consistent with the XANES results.

Transmission electron microscopy (TEM) shows no evidence of Pd-based nanoparticles on the Pd_{SA}-PCN surface (Figure S4). Aberration-corrected high-angle annular dark-field scanning transmission electron microscopy (AC-HAADF-STEM) revealed a uniform distribution of high-density Pd single atoms on the PCN support intuitively, with no apparent nanoparticles observed (Figure 2G). Together with energy-dispersive X-ray spectroscopy (EDS) mapping (Figure 2H), it confirmed the homogeneous presence of Pd, C, and N in the Pd_{SA}-PCN catalyst. Additionally, the band edge position diagrams of Pd_{SA}-PCN and PCN show that incorporation of Pd single atoms modifies the electronic structure of the material: Pd_{SA}-PCN shows a narrower bandgap (2.63 eV) compared to PCN (2.72 eV), with shifts in both the conduction band (CB) and valence band (VB) positions, while its inherent band structure is preserved (Figure 2I; the CB was determined by the Mott–Schottky curve (Figure S6b), and the band gap was obtained from UV–vis DRS spectra (Figure S6c) via the Tauc plot). Importantly, the VB position of Pd_{SA}-PCN (+1.49 V *vs.* SHE) is sufficiently positive to thermodynamically drive water oxidation ($E_{O2/H2O}$ = +1.23 V *vs.* SHE), maintaining the oxidation capability of PCN.

Collectively, these results provide strong evidence for the successful preparation of the UHD single-atom Pd catalyst on the PCN support, with the Pd species existing in a cationic state and uniquely coordinated within the PCN framework.

Investigation of Catalytic Performance in Carbonylative Reductive Coupling. The catalytic performance of Pd_{SA}-PCN in the carbonylative reductive coupling reaction was investigated with iodobenzene (**1a**) as the model aryl iodide substrate. Through comprehensive screening processes, pivaldehyde (**2a**) was identified as the optimal carbonyl source, potassium phosphate as the base (Tables S5–S8), and water served as the reductant in this system. Under the optimized conditions, the desired product **3a** was obtained in 75% isolated yield.

The screening of metal species and their forms on the support revealed that among common transition metals, only palladium exhibited significant catalytic activity (Scheme 1A). The comparison between the single-atom catalyst (Pd_{SA}-PCN) and nanoparticles (Pd_{NP}-PCN) further highlighted the advantage of

https://doi.org/10.1021/jacs.5c12630
J. Am. Chem. Soc. XXXX, XXX, XXX–XXX

Scheme 2. Substrate Scope of Carbonylative Reductive Coupling[a]

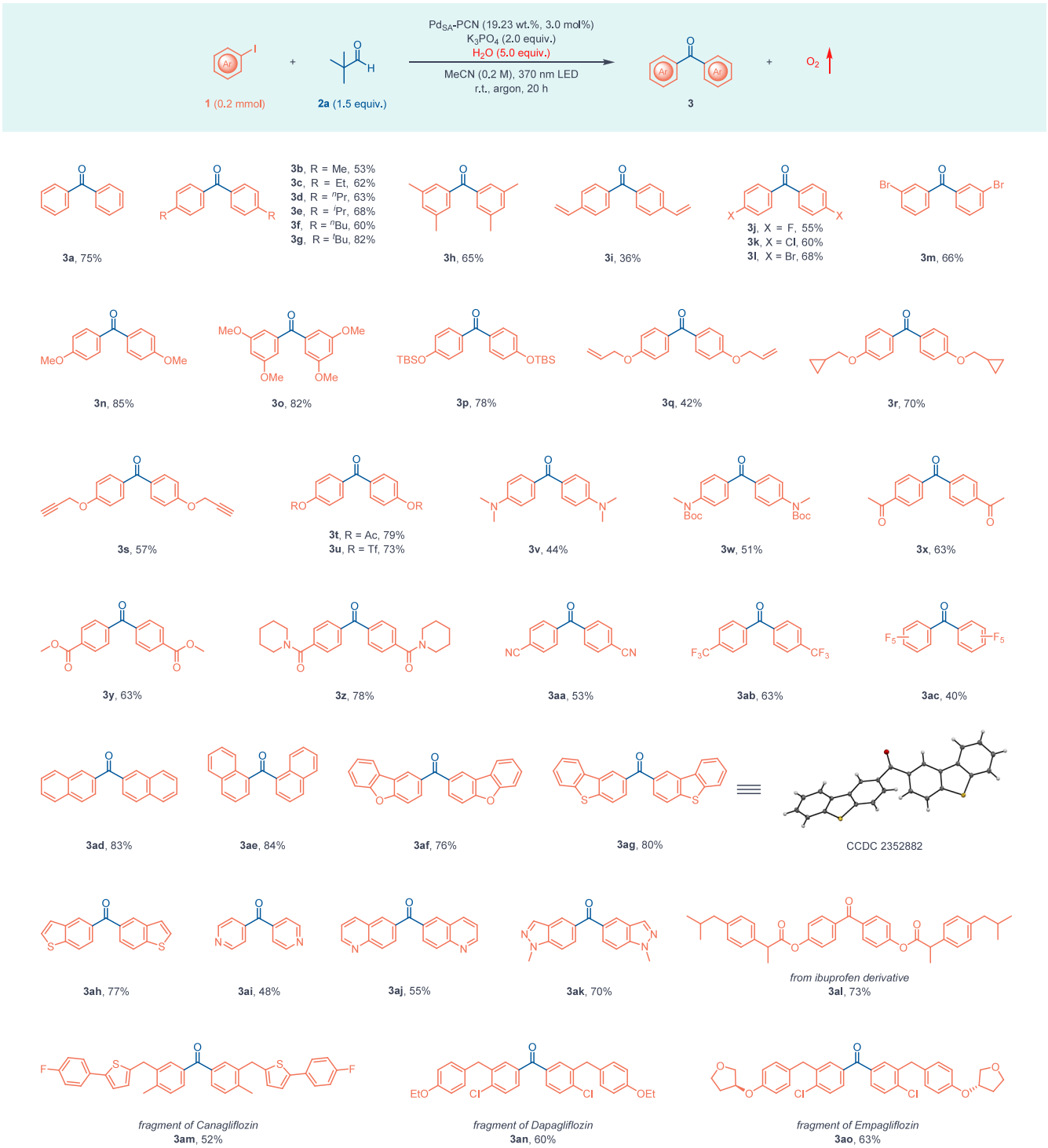

[a]Reactions were conducted under the standard conditions: **1** (0.2 mmol), **2a** (0.3 mmol, 1.5 equiv), Pd_{SA}-PCN (19.23 wt %, 3.3 mg, 3.0 mol %), K_3PO_4 (85 mg, 2.0 equiv), H_2O (18 μL, 5.0 equiv), MeCN (1.0 mL), 370 nm LED (40 W), 20 h, r.t., under an argon atmosphere; isolated yields were given.

single-atom dispersion. Pd_{NP}-PCN demonstrated notably lower activity and produced a significant amount of the biphenyl byproduct (**3a′**), a phenomenon consistent with Zheng's previous findings.[56] One possible reason is the localized surface plasmon resonance (LSPR) effect of palladium nanoparticles, which enhances their reducing capability and facilitates the reduction of iodobenzene to biphenyl.[57−59] Additionally, control experiments using pure PCN without Pd resulted in no product formation, confirming the essential role of Pd single atoms in this reaction. A 370 nm LED proves optimal compared to longer wavelengths (Scheme 1B), and such a phenomenon is compatible with the results of ultraviolet−visible diffuse reflectance spectroscopy (UV−vis DRS) of these catalysts. To further investigate the catalytic performance of Pd_{SA}-PCN, a

https://doi.org/10.1021/jacs.5c12630
J. Am. Chem. Soc. XXXX, XXX, XXX−XXX

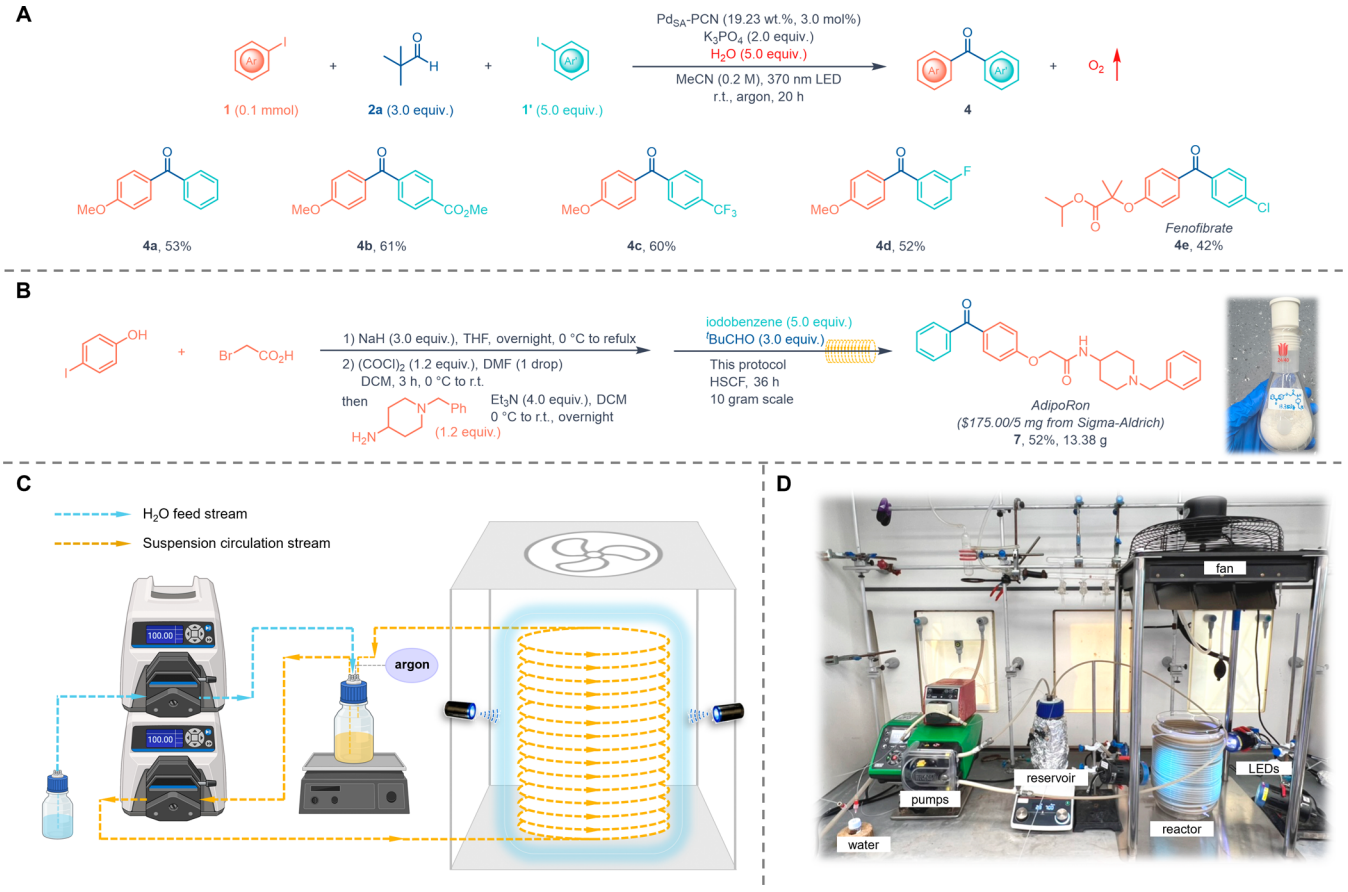

Figure 3. (A) Synthesis of unsymmetrical diaryl ketones. (B) Facile synthesis of AdipoRon. (C) Schematic illustration of the high-speed circulation flow system. (D) Platform setup.

series of control experiments were conducted. Notably, when the amount of metal was kept constant at 3 mol %, reducing the Pd loading while increasing the total amount of the catalyst resulted in a significant decrease in the yield of the desired product **3a** and a concurrent increase in the yield of the byproduct **3a′** (Scheme 1C). This trend suggests that the reaction relies on synergistic catalysis between adjacent Pd sites to transfer CO, thereby favoring the formation of the desired product over the byproduct. Additionally, the absence of water (Table S4) also resulted in no product formation, highlighting its role as a reductant in the reaction system. These results collectively demonstrate the exceptional catalytic performance of high-density Pd$_{SA}$-PCN in the carbonylative reductive coupling reaction, emphasizing the synergistic effect of densely distributed Pd single atoms, the PCN support, water, and light irradiation on achieving high catalytic efficiency.

Utilizing the optimized reaction conditions, we subsequently investigated the scope of this cascade transformation (Scheme 2). The methodology exhibited a remarkable tolerance for a wide array of substituents on the aryl ring. Both meta- and para-alkyl substituents were well-accommodated (**3a**−**3h**). However, sterically hindered ortho-alkyl-substituted aryl iodides were not compatible with the current reaction conditions and failed to provide the desired products. The vinyl-substituted compound **3i** gave a relatively lower yield of 36%, likely due to the susceptibility of the double bond to radicals during the reaction. Aryl iodides bearing fluoro, chloro, or bromo substituents (**3j**−**3m**) smoothly underwent the coupling reaction, while these halogen atoms remained intact, confirming that the reductive coupling was selective for aryl iodides. Electron-rich substrates containing alkoxy groups, silyl ethers (**3n**−**3s**), phenol esters (**3t** and **3u**), and amines (**3v** and **3w**) were also compatible with the reaction conditions. Electron-deficient groups including ketones, esters, amides, nitriles, and trifluoromethyl substituents (**3x**−**3ac**) were also compatible, albeit affording lower yields compared to electron-rich substrates. Notably, even highly electron-deficient substrates such as pentafluoroiodobenzene underwent the desired transformation (**3ac**), underscoring the robustness of our catalytic system. Furthermore, the reaction illustrated good compatibility with polycyclic aromatic compounds (**3ad** and **3ae**) and a diverse array of heterocycles, including dibenzofuran, dibenzothiophene, benzothiophene, pyridine, quinoline, and indazole derivatives with yields up to 84% (**3af**−**3ak**).

To demonstrate the synthetic utility of this methodology, we applied it to the late-stage functionalization of more complex bioactive molecules. An ibuprofen derivative (**3al**) and fragments of several pharmaceutically relevant molecules, including canagliflozin (**3am**), dapagliflozin (**3an**), and empagliflozin (**3ao**), were efficiently transformed, with yields ranging from 52% to 73%. These examples not only highlight the potential of this methodology in pharmaceutical synthesis but also underscore its compatibility with the intricate molecular structures often encountered in drug discovery efforts.

Synthetic Applications. By introducing 5.0 equiv of another aryl iodide, this strategy could be extended to the synthesis of unsymmetrical diaryl ketones (Figure 3A, **4a**−**4d**). Furthermore, this approach was also applicable to the synthesis

https://doi.org/10.1021/jacs.5c12630
J. Am. Chem. Soc. XXXX, XXX, XXX−XXX

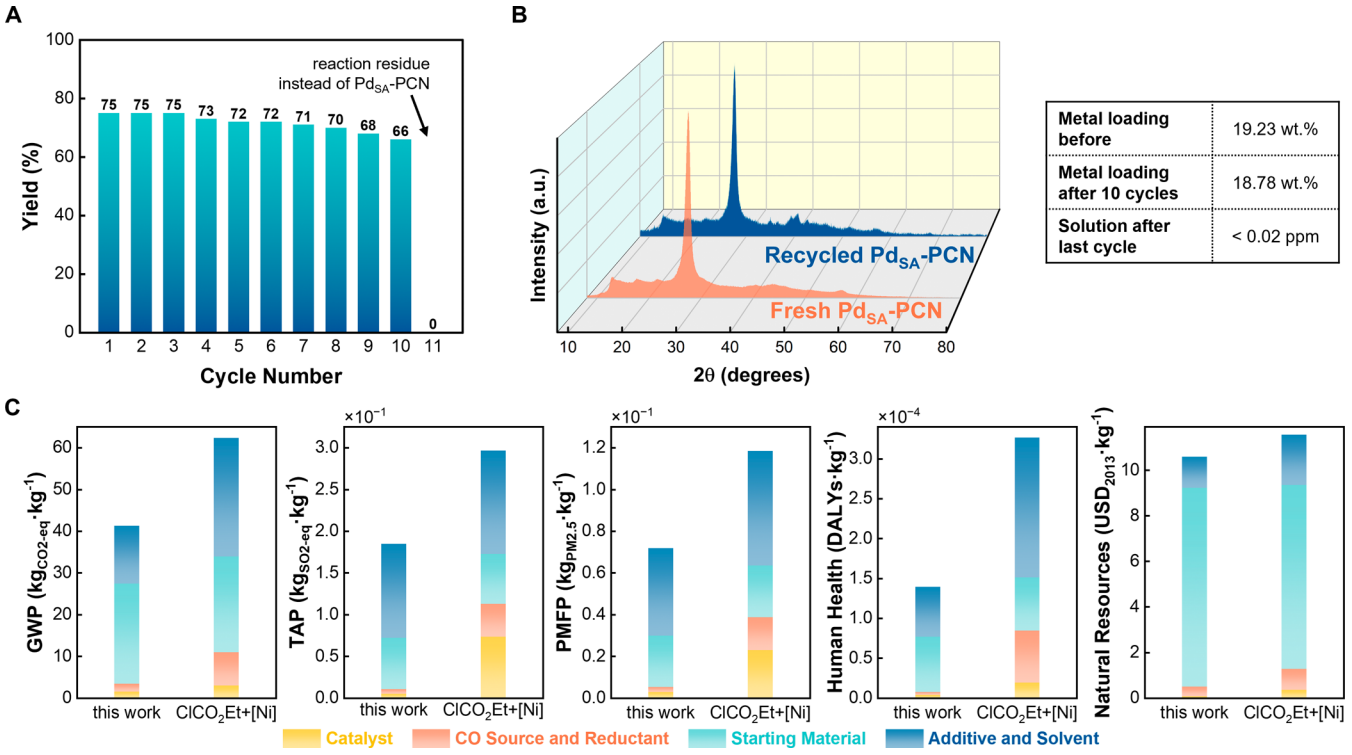

Figure 4. (A) The yield of model reaction was over 10 times of catalyst recycling. (B) XRD spectra of Pd$_{SA}$-PCN and recycled Pd$_{SA}$-PCN and the ICP-OES results. (C) LCA of carbonylative reductive coupling. GWP, global warming potential; TAP, terrestrial acidification potential; PMFP, particulate matter formation potential; DALYs, disability-adjusted life years; USD, U.S. dollars.

of the pharmaceutical compound fenofibrate (**4e**). The synthesis of AdipoRon (**7**) was achieved through a three-step process (Figure 3B). 4-Iodophenol was converted to a carboxylic acid intermediate through an S_N2 reaction, followed by an amidation to give the amide precursor. The last step employed the carbonylative reductive coupling protocol to produce AdipoRon. Notably, we successfully achieved the synthesis of AdipoRon in a decagram scale using a simple in-house-built high-speed circulation flow (HSCF) platform (Figure 3C,D), which tolerated the insoluble photocatalyst and base in a flow fashion.[60] The HSCF system mitigates light attenuation in scale-up by maintaining short optical paths and continuous circulation, ensuring uniform photon flux and avoiding uneven irradiation often observed in traditional batch photoreactors.[61] This process gave 13.38 g of AdipoRon (52% yield), demonstrating the scalability and potential industrial use of our method.

Recycle Experiments and LCA. To evaluate the recyclability and stability of our Pd$_{SA}$-PCN catalyst, we conducted experiments over 10 consecutive reaction cycles (Figure 4A). The results demonstrated the remarkable stability of the catalyst, with the isolated yield only slightly decreasing from 75% in the first cycle to 66% after 10 cycles. This minimal loss of catalytic activity over multiple uses highlighted the robust nature of our SAPC system. Importantly, XRD patterns of the fresh and recycled Pd$_{SA}$-PCN catalysts (Figure 4B) showed no significant differences, with no observable peak characteristic of Pd nanoparticle formation. This indicated that the single-atom dispersion of Pd on the PCN support was largely maintained throughout the recycling process. To further verify the heterogeneous nature of the catalysis, we performed a leaching test by removing the Pd$_{SA}$-PCN catalyst after the 10th cycle and using the filtrate as the catalyst for an additional (11th) reaction. No product formation was observed, indicating that the active species did not leach into the solution. ICP-OES analysis showed that the Pd content slightly decreased from 19.23 to 18.78 wt % after 10 cycles, which can be attributed to the adsorption of reaction species on the catalyst support. Moreover, ICP-OES analysis of the final reaction filtrate confirmed the absence of Pd in solution, further supporting the heterogeneous character of the Pd$_{SA}$-PCN catalyst.

To quantify the environmental impact of our carbonylative reductive coupling strategy, we conducted a comprehensive LCA analysis comparing our approach with the Ni/ClCO$_2$Et/Zn strategy[35] (Figure 4C). The LCA results demonstrate superior environmental performance across all evaluated impact categories, including global warming potential (GWP), terrestrial acidification potential (TAP), particulate matter formation potential (PMFP), human health impacts, and natural resources depletion. These remarkable environmental benefits are attributed to the excellent recyclability and reusability of the Pd$_{SA}$-PCN catalyst, the use of inexpensive pivaldehyde as the carbonyl source, and water as an environmentally benign reductant.

Mechanistic Elucidation with Supporting Evidence. To elucidate the reaction mechanism, we conducted a series of control experiments (Figure 5). Initially, we investigated the byproducts of the reaction (Figure 5A). When **2b** was used as the carbonyl source, the decarbonylative byproduct **2b′** was generated. With $H_2{}^{18}O$ as the starting material, $^{18}O_2$ was also detected via gas chromatography−mass spectrometry (GC-MS), confirming water as the reductant in this reaction. A significantly lower yield (8%) was obtained when we utilized CO gas as the carbonyl source (Figure 5B), which could be attributed to the inefficiency of photomediated gas/liquid/solid three-phase reactions. This result highlights the effectiveness of

https://doi.org/10.1021/jacs.5c12630
J. Am. Chem. Soc. XXXX, XXX, XXX−XXX

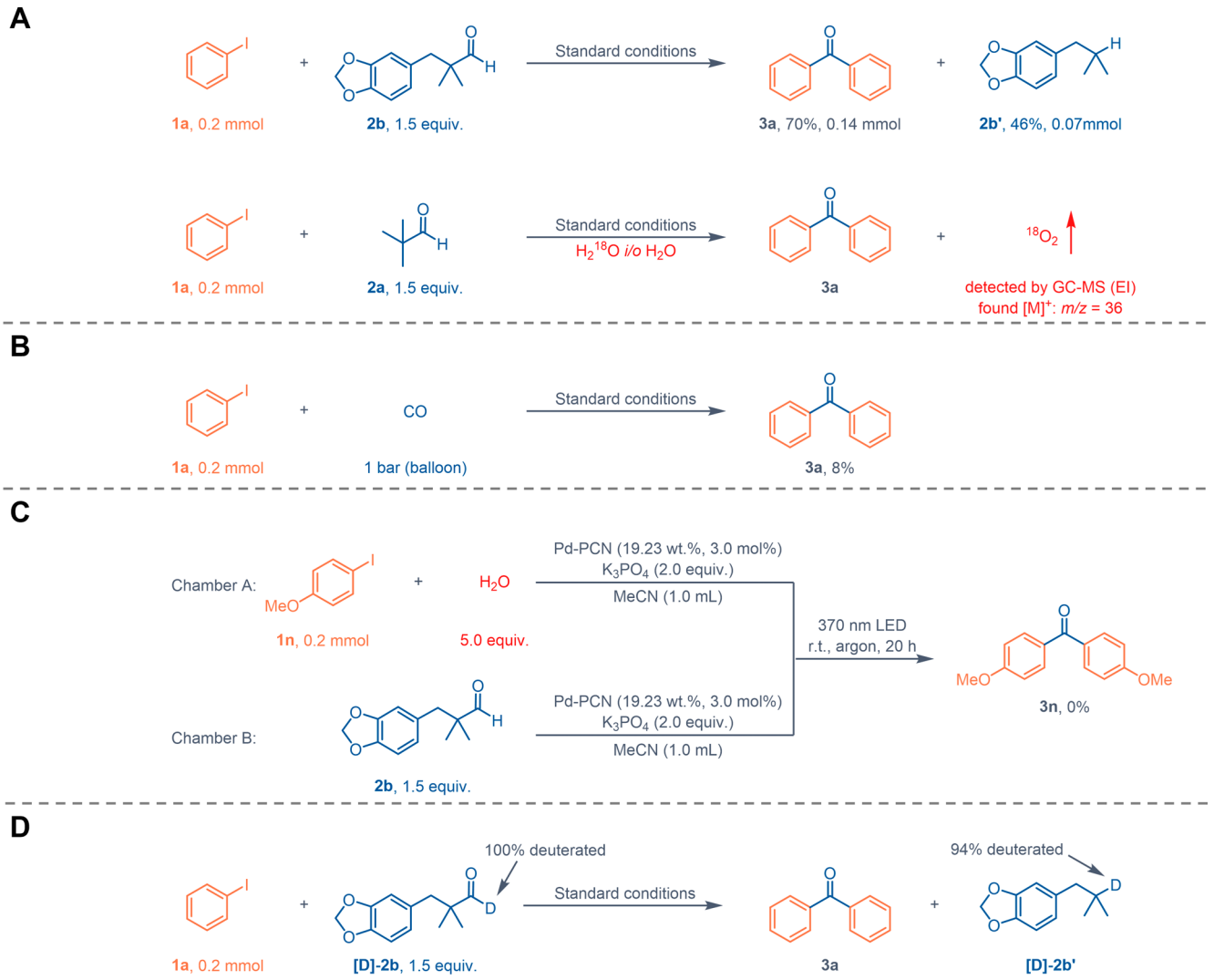

Figure 5. (A) Detection of byproducts. (B) CO gas as the carbonyl source. (C) Two-chamber system experiment. (D) Deuterium-labeling experiment.

in situ generated CO from aldehyde decarbonylation for efficient CO incorporation. Moreover, a two-chamber reactor experiment was conducted to investigate whether the physical separation of the carbonyl source and aryl iodide would affect the reaction (Figure 5C), but no product formation was observed. An isotope-labeling study was conducted using a deuterated aldehyde (Figure 5D). Analysis of the decarbonylative byproduct revealed a 94% deuterium ratio, indicating that the hydrogen atom at the decarbonylation site predominantly originated from the aldehyde.

To elucidate the mechanistic role of the high-density Pd_{SA}-PCN catalyst in the carbonylative reductive coupling reaction, we systematically investigated the cooperative transformation pathway of pivaldehyde, iodobenzene, and water by integrating experimental findings with theoretical studies using density functional theory (DFT) calculations. As illustrated in Figure 6A, the reaction is governed by the synergistic catalytic effect of the vicinal Pd centers. Initially, under light irradiation, the Pd^{II} species are reduced to Pd^{I} by photoelectrons from the PCN support.[39,62] The Pd_1 site then adsorbs pivaldehyde and begins the oxidative addition process, promoting substrate decarbonylation via a subsequent CO deinsertion−reductive elimination pathway, affording isobutane and adsorbed CO (^{3}**IS4**). The Pd_2 site absorbs the iodobenzene and undergoes oxidative addition to form an aryl−Pd−I intermediate (^{3}**IS6**). The presence of K_3PO_4 drives the equilibrium forward via a salting-out effect, promoting dehalogenation and the formation of insoluble KI. Concurrently, electrons on the CB reduce the Pd_2 center to form ^{2}**IS7** (Figure 6B). Subsequently, the aryl group migrates onto the adjacent adsorbed CO ligand, yielding the key Pd−benzoyl intermediate (^{2}**IS8**). Finally, another iodobenzene molecule is adsorbed, and the shuttling process recurs, followed by reductive elimination to furnish the benzophenone product.

Energetically, the overall transformation is thermodynamically spontaneous and kinetically feasible. A moderate energy barrier of 0.32 eV ensures that the reaction proceeds smoothly under mild conditions (Figure 6C) and effectively suppresses side reactions (Figure S14). The synergistic catalysis of Pd_{SA}-PCN arises from a dual "structural−spatial separation + charge−functional separation" mechanism. The catalyst features spatially isolated Pd sites rather than bimetallic species with direct metal−metal bonds, thus preserving the electronic independence of each center. Photoexcitation is pivotal, and time-dependent DFT (TDDFT) calculations reveal a pronounced ligand-to-metal charge transfer (LMCT) character, with excited electrons migrated into the Pd/N centers while holes were

https://doi.org/10.1021/jacs.5c12630
J. Am. Chem. Soc. XXXX, XXX, XXX−XXX

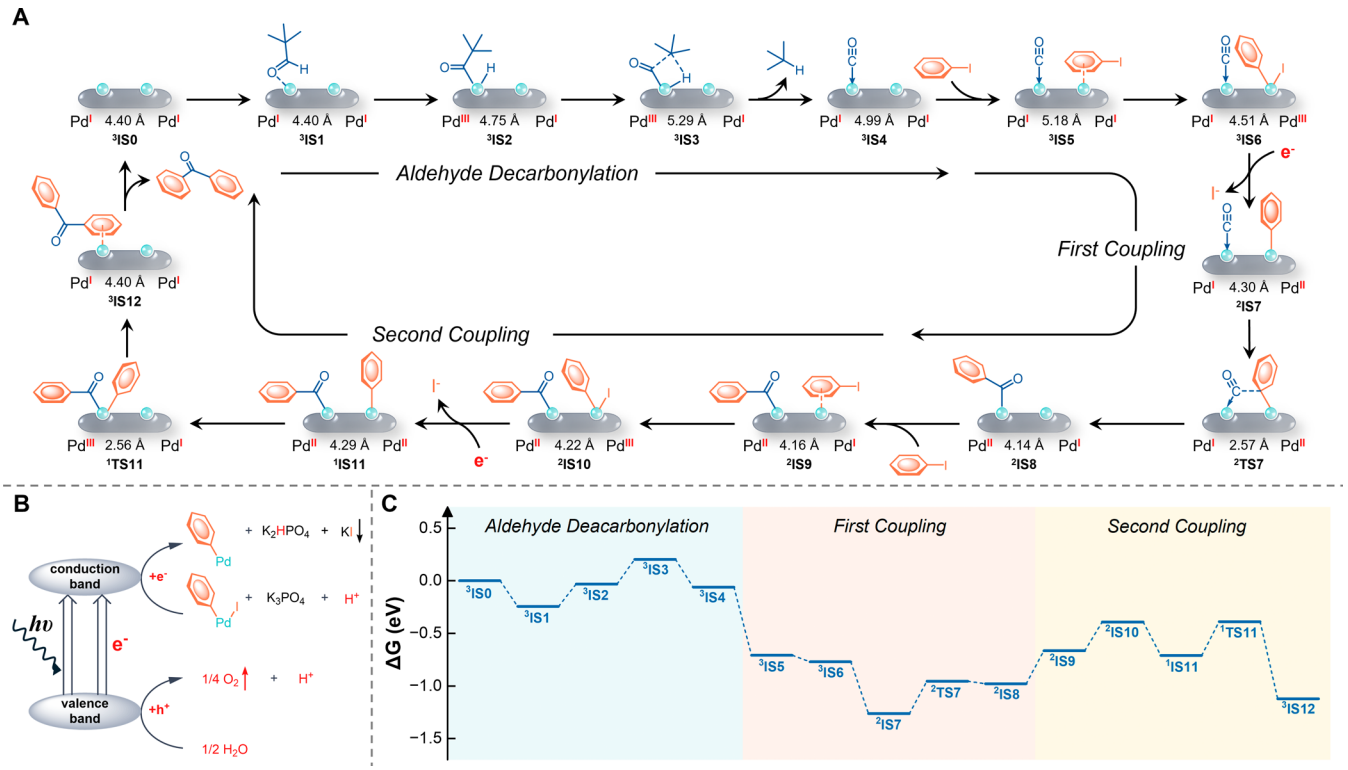

Figure 6. (A) Proposed reaction mechanisms. The arrows and dashed lines denote the dative and covalent bonds, respectively. (B) Schematic diagram of Pd reduction and water oxidation. (C) Calculated energy level diagram for carbonylative reductive coupling. The superscript on the left of each symbol denotes the spin multiplicity.

localized on the PCN framework. This charge separation extends carrier lifetimes and provides an intrinsic electrochemical driving force for the entire relay pathway.

CONCLUSIONS

In summary, we have developed a novel photoinduced single-atom Pd-catalyzed carbonylative reductive coupling reaction utilizing pivaldehyde as an economical and safe carbonyl source, with water serving as an environmentally benign reductant, a strategy validated for its environmental benefits by LCA. This methodology seamlessly integrates decarbonylation, photo-mediated water oxidation, and carbonylative coupling into a single catalytic system. The high-density Pd single atom anchored on a PCN support as the catalyst demonstrates exceptional synergistic catalytic activity, a broad substrate scope, and remarkable recyclability. DFT calculations provided an atomic-level rationale for this synergistic effect. The practical utility of this method was showcased through the efficient synthesis of bioactive compounds, including a decagram scale synthesis of AdipoRon. This protocol not only provides a sustainable approach to valuable ketone compounds but also highlights the potential of a synergistic catalytic effect with a high-density heterogeneous single-atom photocatalyst (SAPC).

ASSOCIATED CONTENT

Supporting Information

The Supporting Information is available free of charge at https://pubs.acs.org/doi/10.1021/jacs.5c12630.

General procedures, catalyst preperations and characterizations, tables of reaction optimizations, calculation details, and characterization data for all the products (PDF)

Accession Codes

Deposition Number 2352882 contains the supplementary crystallographic data for this paper. These data can be obtained free of charge via the joint Cambridge Crystallographic Data Centre (CCDC) and Fachinformationszentrum Karlsruhe Access Structures service.

AUTHOR INFORMATION

Corresponding Authors

Jun Li − *Department of Chemistry and Engineering Research Center of Advanced Rare-Earth Materials of Ministry of Education, Tsinghua University, Beijing 100084, P. R. China; Department of Chemistry, Southern University of Science and Technology, Shenzhen 518055, P. R. China; Fundamental Science Center of Rare Earths, Ganjiang Innovation Academy, Chinese Academy of Sciences, Ganzhou 341000, P. R. China;* orcid.org/0000-0002-8456-3980; Email: junli@tsinghua.edu.cn

Jun-An Ma − *Joint School of National University of Singapore and Tianjin University, International Campus of Tianjin University, Fuzhou 350207, P. R. China; Department of Chemistry, State Key Laboratory of Synthetic Biology, Tianjin University, Tianjin 300072, P. R. China;* orcid.org/0000-0002-3902-6799; Email: majun_an68@tju.edu.cn

Jie Wu − *Department of Chemistry, National University of Singapore, Singapore 117543, Republic of Singapore; National University of Singapore (Suzhou) Research Institute, Suzhou 215123, P. R. China;* orcid.org/0000-0002-9865-180X; Email: chmjie@nus.edu.sg

Authors

Haolin Du − *Joint School of National University of Singapore and Tianjin University, International Campus of Tianjin*

https://doi.org/10.1021/jacs.5c12630
J. Am. Chem. Soc. XXXX, XXX, XXX−XXX

University, Fuzhou 350207, P. R. China; Department of Chemistry, National University of Singapore, Singapore 117543, Republic of Singapore; Department of Chemistry, State Key Laboratory of Synthetic Biology, Tianjin University, Tianjin 300072, P. R. China; orcid.org/0000-0002-2710-1974

Qi Yu − *School of Materials Science and Engineering and Shaanxi Provincial Key Laboratory of Catalysis, Shaanxi University of Technology, Hanzhong 723001, P. R. China*

Yucong Miao − *Department of Chemistry, National University of Singapore, Singapore 117543, Republic of Singapore; State Key Laboratory of Chemical Resource Engineering, Beijing University of Chemical Technology, Beijing 100029, P. R. China*

Junli Ao − *Department of Chemistry, National University of Singapore, Singapore 117543, Republic of Singapore; State Key Laboratory of Functions and Applications of Medicinal Plants & School of Pharmacy, Guizhou Medical University, Gui-an New District, Guizhou 561113, P. R. China;* orcid.org/0000-0002-2437-6059

Jiale Wu − *Department of Chemistry, National University of Singapore, Singapore 117543, Republic of Singapore*

Kun Fu − *School of Materials Science and Engineering and Shaanxi Provincial Key Laboratory of Catalysis, Shaanxi University of Technology, Hanzhong 723001, P. R. China*

Yang Shi − *Department of Chemistry, National University of Singapore, Singapore 117543, Republic of Singapore*

Complete contact information is available at: https://pubs.acs.org/10.1021/jacs.5c12630

Author Contributions

‡Haolin Du and Qi Yu contributed equally.

Notes

The authors declare no competing financial interest.

■ ACKNOWLEDGMENTS

We acknowledge financial support from the Prime Minister's Office of Singapore under its NRF-CRP Programme (NRF-CRP29-2022-0004), Agency for Science, Technology and Research (A*STAR) under its MTC IRG Grant (Project M22K2c0082), financial support from Pfizer (A-8002093-00-00), National Natural Science Foundation of China (22371200, 92156025, and 22473071), NUS (Suzhou) Research Institute, Science and Technology Project of Jiangsu Province (BZ2022056), and NSFC Center for Single-Atom Catalysis (No. 22388102). We are grateful to Prof. Jiong Lu (NUS) and Prof. Xiao Hai (PKU) for their assistance on catalyst preparation and insightful discussions.

■ REFERENCES

(1) Ni, J.; Xia, X.; Gu, D.; Wang, Z. Ti-Catalyzed Modular Ketone Synthesis from Carboxylic Derivatives and Gem-Dihaloalkanes. *J. Am. Chem. Soc.* **2023**, *145*, 14884−14893.

(2) Foley, D. J.; Waldmann, H. Ketones as Strategic Building Blocks for the Synthesis of Natural Product-Inspired Compounds. *Chem. Soc. Rev.* **2022**, *51*, 4094−4120.

(3) Liu, B.; Hu, F.; Shi, B.-F. Recent Advances on Ester Synthesis via Transition-Metal Catalyzed C-H Functionalization. *ACS Catal.* **2015**, *5*, 1863−1881.

(4) Cook, A.; Prakash, S.; Zheng, Y.-L.; Newman, S. G. Exhaustive Reduction of Esters Enabled by Nickel Catalysis. *J. Am. Chem. Soc.* **2020**, *142*, 8109−8115.

(5) Faculak, M. S.; Veatch, A. M.; Alexanian, E. J. Cobalt-Catalyzed Synthesis of Amides from Alkenes and Amines Promoted by Light. *Science* **2024**, *383*, 77−81.

(6) Schoenberg, A.; Bartoletti, I.; Heck, R. F. Palladium-Catalyzed Carboalkoxylation of Aryl, Benzyl, and Vinylic Halides. *J. Org. Chem.* **1974**, *39*, 3318−3326.

(7) Schoenberg, A.; Heck, R. F. Palladium-Catalyzed Amidation of Aryl, Heterocyclic, and Vinylic Halides. *J. Org. Chem.* **1974**, *39*, 3327−3331.

(8) Schoenberg, A.; Heck, R. F. Palladium-Catalyzed Formylation of Aryl, Heterocyclic, and Vinylic Halides. *J. Am. Chem. Soc.* **1974**, *96*, 7761−7764.

(9) Echavarren, A. M.; Stille, J. K. Palladium-Catalyzed Carbonylative Coupling of Aryl Triflates with Organostannanes. *J. Am. Chem. Soc.* **1988**, *110*, 1557−1565.

(10) Bai, Y.; Davis, D. C.; Dai, M. Natural Product Synthesis via Palladium-Catalyzed Carbonylation. *J. Org. Chem.* **2017**, *82*, 2319−2328.

(11) Brennführer, A.; Neumann, H.; Beller, M. Palladium-Catalyzed Carbonylation Reactions of Aryl Halides and Related Compounds. *Angew. Chem., Int. Ed.* **2009**, *48*, 4114−4133.

(12) Wu, X.-F.; Neumann, H.; Beller, M. Palladium-Catalyzed Carbonylative Coupling Reactions between Ar−X and Carbon Nucleophiles. *Chem. Soc. Rev.* **2011**, *40*, 4986−5009.

(13) Fusano, A.; Sumino, S.; Nishitani, S.; Inouye, T.; Morimoto, K.; Fukuyama, T.; Ryu, I. Pd/Light-Accelerated Atom-Transfer Carbonylation of Alkyl Iodides: Applications in Multicomponent Coupling Processes Leading to Functionalized Carboxylic Acid Derivatives. *Chem. − Eur. J.* **2012**, *18*, 9415−9422.

(14) Sumino, S.; Fusano, A.; Fukuyama, T.; Ryu, I. Carbonylation Reactions of Alkyl Iodides through the Interplay of Carbon Radicals and Pd Catalysts. *Acc. Chem. Res.* **2014**, *47*, 1563−1574.

(15) Matsubara, H.; Kawamoto, T.; Fukuyama, T.; Ryu, I. Applications of Radical Carbonylation and Amine Addition Chemistry: 1,4-Hydrogen Transfer of 1-Hydroxylallyl Radicals. *Acc. Chem. Res.* **2018**, *51*, 2023−2035.

(16) Torres, G. M.; Liu, Y.; Arndtsen, B. A. A Dual Light-Driven Palladium Catalyst: Breaking the Barriers in Carbonylation Reactions. *Science* **2020**, *368*, 318−323.

(17) Chen, G.; Zhou, R.; Zhang, X.; Xiao, X.; Kramer, S.; Cheng, G.-J.; Lian, Z. Carbonylative Cross-Electrophile Coupling between Aryl Bromides and Aryl Triflates Enabled by Palladium and Rhodium Cooperative Catalysis and CO as Reductant. *ACS Catal.* **2022**, *12*, 14582−14591.

(18) Zhang, Y.; Cao, Q.; Xi, Y.; Wu, X.; Qu, J.; Chen, Y. Nickel-Catalyzed Carbonylative Negishi Cross-Coupling of Unactivated Secondary Alkyl Electrophiles with 1 atm CO Gas. *J. Am. Chem. Soc.* **2024**, *146*, 7971−7978.

(19) Hermange, P.; Lindhardt, A. T.; Taaning, R. H.; Bjerglund, K.; Lupp, D.; Skrydstrup, T. Ex Situ Generation of Stoichiometric and Substoichiometric ^{12}CO and ^{13}CO and Its Efficient Incorporation in Palladium Catalyzed Aminocarbonylations. *J. Am. Chem. Soc.* **2011**, *133*, 6061−6071.

(20) Friis, S. D.; Taaning, R. H.; Lindhardt, A. T.; Skrydstrup, T. Silacarboxylic Acids as Efficient Carbon Monoxide Releasing Molecules: Synthesis and Application in Palladium-Catalyzed Carbonylation Reactions. *J. Am. Chem. Soc.* **2011**, *133*, 18114−18117.

(21) Etemadi-Davan, E.; Iranpoor, N. $Cr(CO)_6$ Mediated Carbonylative Homo-Coupling of Aryl Iodides: Direct Access to Symmetrical Diarylketones. *ChemistrySelect* **2016**, *1*, 4300−4304.

(22) Åkerbladh, L.; Odell, L. R.; Larhed, M. Palladium-Catalyzed Molybdenum Hexacarbonyl-Mediated Gas-Free Carbonylative Reactions. *Synlett* **2019**, *30*, 141−155.

(23) Morimoto, T.; Kakiuchi, K. Evolution of Carbonylation Catalysis: no Need for Carbon Monoxide. *Angew. Chem., Int. Ed.* **2004**, *43*, 5580−5588.

(24) Hansen, S. V. F.; Ulven, T. Oxalyl Chloride as a Practical Carbon Monoxide Source for Carbonylation Reactions. *Org. Lett.* **2015**, *17*, 2832−2835.

(25) Ueda, T.; Konishi, H.; Manabe, K. Palladium-Catalyzed Reductive Carbonylation of Aryl Halides with *N*-Formylsaccharin as a CO Source. *Angew. Chem., Int. Ed.* **2013**, *52*, 8611−8615.
(26) Wang, J.; Yin, Y.; He, X.; Duan, Q.-L.; Bai, R.; Shi, H.-W.; Shi, R. Nickel-Catalyzed Highly Selective Reductive Carbonylation Using Oxalyl Chloride as the Carbonyl Source. *ACS Catal.* **2023**, *13*, 8161−8168.
(27) Singh Chauhan, A.; Kumar, A.; Kumar Sharma, A.; Das, P. Pd-Catalysed Decarbonylation Free Approach to Carbonylative Esterification of 5-HMF to Its Aryl Esters Synthesis Using Aryl Halides and Oxalic Acid as C1 Source. *Chem. − Eur. J.* **2021**, *27*, 12971−12975.
(28) Shao, C.; Lu, A.; Wang, X.; Zhou, B.; Guan, X.; Zhang, Y. Oxalic Acid as the *in situ* Carbon Monoxide Generator in Palladium-Catalyzed Hydroxycarbonylation of Arylhalides. *Org. Biomol. Chem.* **2017**, *15*, 5033−5040.
(29) Yin, Z.; Wu, X.-F. The Design of an *in*−*ex* Tube for Gas Related Organic Reactions. *Org. Process Res. Dev.* **2017**, *21*, 1869−1871.
(30) Friis, S. D.; Lindhardt, A. T.; Skrydstrup, T. The Development and Application of Two-Chamber Reactors and Carbon Monoxide Precursors for Safe Carbonylation Reactions. *Acc. Chem. Res.* **2016**, *49*, 594−605.
(31) Tien, C.-H.; Trofimova, A.; Holownia, A.; Kwak, B. S.; Larson, R. T.; Yudin, A. K. Carboxyboronate as a Versatile *in situ* CO Surrogate in Palladium-Catalyzed Carbonylative Transformations. *Angew. Chem., Int. Ed.* **2021**, *60*, 4342−4349.
(32) De La Cruz, L. K.; Bauer, N.; Cachuela, A.; Tam, W. S.; Tripathi, R.; Yang, X.; Wang, B. Light-Activated CO Donor as a Universal CO Surrogate for Pd-Catalyzed and Light-Mediated Carbonylation. *Org. Lett.* **2022**, *24*, 4902−4907.
(33) Le, Z.; Ying, J.; Wu, X.-F. More than a CO Source: Palladium-Catalyzed Carbonylative Synthesis of Butenolides from Propargyl Alcohols and TFBen. *Org. Chem. Front.* **2019**, *6*, 3158−3161.
(34) Fu, L.-Y.; Ying, J.; Qi, X.; Peng, J.-B.; Wu, X.-F. Palladium-Catalyzed Carbonylative Synthesis of Isoindolinones from Benzylamines with TFBen as the CO Source. *J. Org. Chem.* **2019**, *84*, 1421−1429.
(35) Shi, R.; Hu, X. From Alkyl Halides to Ketones: Nickel-Catalyzed Reductive Carbonylation Utilizing Ethyl Chloroformate as the Carbonyl Source. *Angew. Chem., Int. Ed.* **2019**, *58*, 7454−7458.
(36) Chen, H.; Yue, H.; Zhu, C.; Rueping, M. Reactivity in Nickel-Catalyzed Multi-Component Sequential Reductive Cross-Coupling Reactions. *Angew. Chem., Int. Ed.* **2022**, *61*, No. e202204144.
(37) Wang, L.; Wang, H.; Lu, J. Local Chemical Environment Effect in Single-Atom Catalysis. *Chem. Catal.* **2023**, *3*, No. 100492.
(38) Chen, F.; Jiang, X.; Zhang, L.; Lang, R.; Qiao, B. Single-Atom Catalysis: Bridging the Homo- and Heterogeneous Catalysis. *Chin. J. Catal.* **2018**, *39*, 893−898.
(39) Vijeta, A.; Casadevall, C.; Roy, S.; Reisner, E. Visible-Light Promoted C-O Bond Formation with an Integrated Carbon Nitride-Nickel Heterogeneous Photocatalyst. *Angew. Chem., Int. Ed.* **2021**, *60*, 8494−8499.
(40) Zhao, X.; Deng, C.; Meng, D.; Ji, H.; Chen, C.; Song, W.; Zhao, J. Nickel-Coordinated Carbon Nitride as a Metallaphotoredox Platform for the Cross-Coupling of Aryl Halides with Alcohols. *ACS Catal.* **2020**, *10*, 15178−15185.
(41) Kwak, M.; Bok, J.; Lee, B.-H.; Kim, J.; Seo, Y.; Kim, S.; Choi, H.; Ko, W.; Antink, W. H.; Lee, C. W.; Yim, G. H.; Seung, H.; Park, C.; Lee, K.-S.; Kim, D.-H.; Hyeon, T.; Yoo, D. Ni Single Atoms on Carbon Nitride for Visible-Light-Promoted Full Heterogeneous Dual Catalysis. *Chem. Sci.* **2022**, *13*, 8536−8542.
(42) Bajada, M. A.; Di Liberto, G.; Tosoni, S.; Ruta, V.; Mino, L.; Allasia, N.; Sivo, A.; Pacchioni, G.; Vilé, G. Light-Driven C-O Coupling of Carboxylic Acids and Alkyl Halides over a Ni Single-Atom Catalyst. *Nat. Synth.* **2023**, *2*, 1092−1103.
(43) Liu, L.; Corma, A. Metal Catalysts for Heterogeneous Catalysis: from Single Atoms to Nanoclusters and Nanoparticles. *Chem. Rev.* **2018**, *118*, 4981−5079.
(44) Wang, A.; Li, J.; Zhang, T. *Heterogeneous Single-Atom Catalysis. Nat. Rev. Chem.* **2018**, *2*, 65−81.
(45) Li, X.; Yang, X.; Zhang, J.; Huang, Y.; Liu, B. In situ/Operando Techniques for Characterization of Single-Atom Catalysts. *ACS Catal.* **2019**, *9*, 2521−2531.
(46) Li, H.; Wang, L.; Dai, Y.; Pu, Z.; Lao, Z.; Chen, Y.; Wang, M.; Zheng, X.; Zhu, J.; Zhang, W.; Si, R.; Ma, C.; Zeng, J. Synergetic Interaction between Neighbouring Platinum Monomers in CO_2 Hydrogenation. *Nat. Nanotechnol.* **2018**, *13*, 411−417.
(47) Hai, X.; Zheng, Y.; Yu, Q.; Guo, N.; Xi, S.; Zhao, X.; Mitchell, S.; Luo, X.; Tulus, V.; Wang, M.; Sheng, X.; Ren, L.; Long, X.; Li, J.; He, P.; Lin, H.; Cui, Y.; Peng, X.; Shi, J.; Wu, J.; Zhang, C.; Zou, R.; Guillén-Gosálbez, G.; Pérez-Ramírez, J.; Koh, M. J.; Zhu, Y.; Li, J.; Lu, J. Geminal-Atom Catalysis for Cross-Coupling. *Nature* **2023**, *622*, 754−760.
(48) Wang, X.; Maeda, K.; Thomas, A.; Takanabe, K.; Xin, G.; Carlsson, J. M.; Domen, K.; Antonietti, M. A Metal-Free Polymeric Photocatalyst for Hydrogen Production from Water under Visible Light. *Nat. Mater.* **2009**, *8*, 76−80.
(49) Thomas, J. M. Tens of Thousands of Atoms Replaced by One. *Nature* **2015**, *525*, 325−326.
(50) Vilé, G.; Albani, D.; Nachtegaal, M.; Chen, Z.; Dontsova, D.; Antonietti, M.; López, N.; Pérez-Ramírez, J. A Stable Single-Site Palladium Catalyst for Hydrogenations. *Angew. Chem., Int. Ed.* **2015**, *54*, 11265−11269.
(51) Gao, G.; Jiao, Y.; Waclawik, E. R.; Du, A. Single Atom (Pd/Pt) Supported on Graphitic Carbon Nitride as an Efficient Photocatalyst for Visible-Light Reduction of Carbon Dioxide. *J. Am. Chem. Soc.* **2016**, *138*, 6292−6297.
(52) Li, Z.; Wang, D.; Wu, Y.; Li, Y. Recent Advances in the Precise Control of Isolated Single-Site Catalysts by Chemical Methods. *Natl. Sci. Rev.* **2018**, *5*, 673−689.
(53) Allasia, N.; Xu, S.; Jafri, S. F.; Borfecchia, E.; Cipriano, L. A.; Terraneo, G.; Tosoni, S.; Mino, L.; Di Liberto, G.; Pacchioni, G.; Vilé, G. Resolving the Nanostructure of Carbon Nitride-Supported Single-Atom Catalysts. *Small* **2025**, *21*, No. 2408286.
(54) Li, X.; Bi, W.; Zhang, L.; Tao, S.; Chu, W.; Zhang, Q.; Luo, Y.; Wu, C.; Xie, Y. Single-Atom Pt as Co-Catalyst for Enhanced Photocatalytic H2 Evolution. *Adv. Mater.* **2016**, *28*, 2427−2431.
(55) Hai, X.; Xi, S.; Mitchell, S.; Harrath, K.; Xu, H.; Akl, D. F.; Kong, D.; Li, J.; Li, Z.; Sun, T.; Yang, H.; Cui, Y.; Su, C.; Zhao, X.; Li, J.; Pérez-Ramírez, J.; Lu, J. Scalable Two-Step Annealing Method for Preparing Ultra-High-Density Single-Atom Catalyst Libraries. *Nat. Nanotechnol.* **2022**, *17*, 174−181.
(56) Tian, X.; Guo, Y.; An, W.; Ren, Y.-L.; Qin, Y.; Niu, C.; Zheng, X. Coupling Photocatalytic Water Oxidation with Reductive Transformations of Organic Molecules. *Nat. Commun.* **2022**, *13*, 6186.
(57) Zhao, J.; Xue, S.; Ji, R.; Li, B.; Li, J. Localized Surface Plasmon Resonance for Enhanced Electrocatalysis. *Chem. Soc. Rev.* **2021**, *50*, 12070−12097.
(58) Zhang, J.; Guan, B.; Wu, X.; Chen, Y.; Guo, J.; Ma, Z.; Bao, S.; Jiang, X.; Chen, L.; Shu, K.; Dang, H.; Guo, Z.; Li, Z.; Huang, Z. Research on Photocatalytic CO_2 Conversion to Renewable Synthetic Fuels Based on Localized Surface Plasmon Resonance: Current Progress and Future Perspectives. *Catal. Sci. Technol.* **2023**, *13*, 1932−1975.
(59) Jiang, J.; Wang, X.; Guo, H. Enhanced Interfacial Charge Transfer/Separation By LSPR-Induced Defective Semiconductor Toward High CO_2RR Performance. *Small* **2023**, *19*, No. 2301280.
(60) Liu, C.; Song, L.; Liu, Q.; Chen, W.; Xu, J.; Wang, M.; Zhang, Y.; Tan, T. W.; Lei, Z.; Cheng, L.; Khan, S. A.; Wu, J. High-Speed Circulation Flow Platform Facilitating Practical Large-Scale Heterogeneous Photocatalysis. *Org. Process Res. Dev.* **2024**, *28*, 1964−1970.
(61) Zondag, S. D. A.; Schuurmans, J. H. A.; Chaudhuri, A.; Visser, R. P. L.; Soares, C.; Padoin, N.; Kuijpers, K. P. L.; Dorbec, M.; van der Schaaf, J.; Noël, T. Determining Photon Flux and Effective Optical Path Length in Intensified Flow Photoreactors. *Nat. Chem. Eng.* **2024**, *1*, 462−471.
(62) Ye, L.-W.; Hu, H.-S.; Schwarz, W. H. E.; Li, J. Physical Origin and Periodicity of the Highest Oxidation States in Heavy-Element Chemistry. *Acc. Chem. Res.* **2025**, *58*, 1903−1912.

https://doi.org/10.1021/jacs.5c12630
J. Am. Chem. Soc. XXXX, XXX, XXX−XXX